Research Square

Preprints are preliminary reports that have not undergone peer review.
They should not be considered conclusive, used to inform clinical practice,
or referenced by the media as validated information.

A Polyimide Hydrodynamic Flow-Focusing Microfluidic Platform for Damage-Mitigated Hard X-ray Absorption Spectroscopy of Aqueous Samples

Pushparani Micheal Raj
MAX IV Laboratory
Yang Chen
MAX IV Laboratory
Laurent Barbe
Uppsala University
Susan Nehzati
MAX IV Laboratory
Ann Terry
MAX IV Laboratory
Anna Fornell
MAX IV Laboratory
Maria Tenje
Uppsala University
Ross Friel
ross.friel@hh.se
Halmstad University
Kajsa G. V. Sigfridsson Clauss
MAX IV Laboratory

Article

Keywords: X-ray spectroscopy, synchrotron, copper K-edge, radiation damage, microfluidics, hydrodynamic flow focusing

Posted Date: July 13th, 2026

DOI: https://doi.org/10.21203/rs.3.rs-10226449/v1

License: This work is licensed under a Creative Commons Attribution 4.0 International License.
Read Full License

Additional Declarations: No competing interests reported.

A Polyimide Hydrodynamic Flow-Focusing Microfluidic Platform for Damage-Mitigated Hard X-ray Absorption Spectroscopy of Aqueous Samples

Pushparani Micheal Raj[1], Yang Chen[1], Laurent Barbe[2], Susan Nehzati[1], Ann Terry[1], Anna Fornell[1], Maria Tenje[2,3], Ross Friel[4], Kajsa G. V. Sigfridsson Clauss*[1]*

[1]MAX IV Laboratory, Lund University, Lund, Sweden

[2]Department of Materials Science and Engineering, Uppsala University, Uppsala, Sweden

[3]Science for Life Laboratory, Uppsala University, Uppsala, Sweden

[4]School of Information Technology, Halmstad University, Halmstad, Sweden

*** Corresponding Authors**

E-mail: ross.friel@hh.se

kajsa.sigfridsson_clauss@maxiv.lu.se

Keywords: *X*-ray spectroscopy, synchrotron, copper *K*-edge, radiation damage, microfluidics, hydrodynamic flow focusing

Abstract

Hard X-ray Absorption Spectroscopy (XAS) is a method to probe the *K*- or *L*-edge of metals. Thus, it is an excellent tool for investigating the coordination of metal ions in solutions. Modern synchrotron beamlines provide a wide range of tuneable X-ray energies with a high flux of photons for analysing many different elements. A disadvantage of the high flux X-rays is the degradation of the sample even after only a brief time of exposure, particularly when samples are static. Microfluidic flow devices offer a wide range of benefits for analysing samples in solutions using XAS. One significant benefit is that they offer constant replenishment of fresh samples to avoid X-ray-induced redox processes, resulting in bubble formation, elevated temperatures and in turn sample degradation. In this work, we analysed $CuSO_4$ in aqueous solutions using XAS and hydrodynamic flow focusing of sample with sheath fluids. X-ray transparent polyimide, low background, microfluidic device (MfD) was fabricated and validated at the Balder beamline in MAX IV synchrotron facility, Sweden. The device was fully functional, and no radiation damage was evident under flow, enabling effective analysis without the sample degradation typically associated with high-flux X-ray exposure. This advancement supports more reliable and efficient XAS studies of metal ions in solution, offering benefits for research in areas such as catalysis and life sciences.

1 Introduction

X-ray absorption Spectroscopy (XAS) is a well-established technique to study the local geometric and/or electron structure of matter[1]. Synchrotron, hard X-ray sources provide an extensive range of X-ray tunability, and 4th generation synchrotrons (such as MAX IV) provide higher brilliance, lower divergence, and higher coherence levels than any previous-generation

synchrotron [2]. However, these properties are coupled with a higher X-ray photon flux on the samples. This leads to faster and/or more extensive degradation of samples being analysed when static samples are exposed for longer times [3–5]. To overcome this, samples must be replenished quickly, accurately and in a setup that minimally interferes with the high-brilliance X-rays from the newest generation synchrotron sources.

Cu^{II} in water containing samples is especially prone to X-ray induced reduction [11]. Water undergoes radiolysis in the X-ray beam with the production of radicals, aqueous electrons, and hydrogen gas. The aqueous electrons in the solution can readily reduce high valent ions, like the Cu^{II} to Cu^{I}. This reduction is particularly easy to follow with XAS by looking at the Cu K-edge XANES, where a pronounced pre-edge peak grows in at ~8980 -8985 eV with increased radiation time. This process is observed at both ambient and cryogenic conditions, but cooling the solution slows down the process. In Gerbrand Mesu et al [3] they investigated different salt solutions at ambient conditions and saw very rapid reduction in the presence of halides ($CuCl_2$, $CuBr_2$), while the sulphate and nitrate salts where stable under their conditions (bending magnet beamline, 0.5 x 0.5 mm^2 beam spot). In this paper we used Cu sulphate salt solution and a much higher flux density on the sample (wiggler beamline, 0.05 x 0.05 mm^2 beam spot size) and could indeed observe similar photoreduction under static conditions. In Nienaber [12] they investigated the photoreduction of salt solutions under cryogenic conditions and monitored the influence of cryoprotectant, but also confirmed that excitation of the edge itself was not important for the reduction effect by radiating the solution below and above the absorption edge.

The use of continuous flow avoids radiation damage with the regularly exchanged samples which are only exposed to the high intense beam for a brief time. However, two common

challenges while using hard X-rays (typically regarded as energy > 3 keV) analysis for aqueous samples are,

- Correct sample presentation within the X-ray source, and
- The necessary replenishment of radiation degraded sample [13].

Microfluidics is one tool that can be integrated into many different [10,14] analytical techniques, suitable to reduce X-ray-induced damage and to enable liquid-phase spectroscopy at synchrotron facilities. Some previously published examples include jet-based flow measurements for tender X-ray spectroscopy, laminar-flow microfluidics combined with soft X-ray absorption spectroscopy, droplet-based microfluidic XAS, and X-ray-compatible microfluidic platforms for in situ synchrotron studies of reacting aqueous systems [6–9]. Recent reviews further show that device material, X-ray path length, background scattering, wall interactions and sample consumption remain central design constraints for X-ray-compatible microfluidics [10]. In contrast to many previously reported hard-XAS liquid-flow systems, the present platform combines an X-ray-transparent, low-background polyimide device with two-dimensional hydrodynamic flow focusing. This allows the sample stream to be confined between sheath flows, positioned away from the channel walls, and tuned in width/path length by adjusting the relative flow rates. The resulting platform provides controlled sample presentation in the X-ray beam while reducing wall interactions, sample consumption, and beam-induced damage.

Here, we present a microfluidic system utilising the principles for hydrodynamic flow focusing [15,16] (see Figure 1) to achieve this. A common method of flow focusing is the lamination of a sample between two streams of a low miscible, non-sample containing fluid [7,17]. The achievement of flow focusing, and the resultant flow volumes are obtained through careful control of the inlet flow rates/pressure and the microfluidic device (MfD) fluidic pathway

design. The device and pressure settings must be matched with the fluid properties; the flow focusing is typically done via empirical methods [18]. In laminar flow regime, the flow velocity approaches to 'zero' at the channel walls, this is considered a primary reason for sample adsorption and reduction at the walls when exposed to X-ray beam [19,20]. Flowing liquids adjacently to achieve flow focusing thus provides a means to avoiding the effects encountered at the wall to liquid interaction by isolating the sample liquid from the device wall [3,9,10].

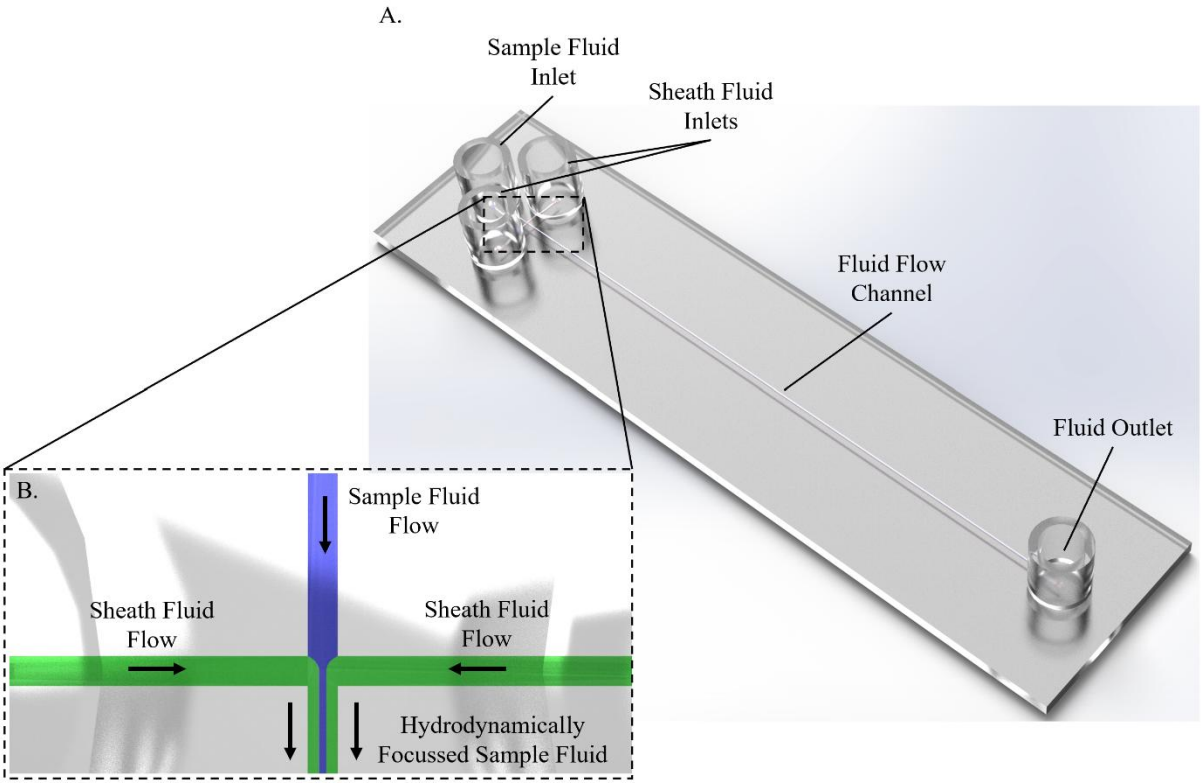


Figure 1 - Hydrodynamic Flow Focusing: A. Typical hydrodynamic flow-focusing microfluidic device showing two sheath fluid inlets and one sample fluid inlet that would be connected to a syringe or microfluidic pump. There is a fluid outlet for collection of the combined sheath and sample B. A close-up shows the focusing of the sample fluid flow by the sheath flows and the resultant "laminated" fluid flow.

Hard-XAS measurements of aqueous metal-ion solutions at high-flux synchrotron beamlines are particularly sensitive to beam-induced chemistry and sample-environment artefacts. In this work, we present a two-dimensional hydrodynamic flow-focusing microfluidic device

fabricated from X-ray-transparent polyimide and designed to minimise background, avoid beam interaction with channel walls, and enable tuneable control of the effective sample width and path length. Using aqueous $CuSO_4$ as a benchmark radiation-sensitive system, we validate the device at the Balder beamline at MAX IV and quantify the trade-off between focused-stream geometry, spectral quality and sample consumption [9,10] demonstrating a novel system for hard-XAS validation of a simple, low-background, wall-isolating polyimide platform for radiation-sensitive aqueous samples.

2 Materials and Methods

2.1 Device Design and Fabrication

Pre-studies were carried out using commercially available Cyclic olefin copolymer (COC) MfDs, which were tested using a $CuSO_4$(aq) sample fluid. Using the Balder XAS beamline at MAX IV Laboratory a long-time-frame data collection was carried out. After three hours of X-ray beam interaction with the COC device at the same spot on the channel it was noted that channel deformation was occurring followed by a heat build-up at the X-ray spot location. It was found that consecutive Cu *K*-edge spectra that were measured in the COC chip displayed changes upon subsequent scans (Figure S1). The authors attribute these spectral changes to a reduction of Cu^{II} to Cu^{I}/Cu^{0} upon the second and third scan. This Cu reduction was determined as being at the location of the X-ray/MfD/solution interaction point [3]. This pre-study led to the design determination that the X-ray beam should not interact with the slower flow along the walls. Therefore, a sheath fluid should achieve a hydrodynamic flow focus removing much of the interaction of the sample fluid from the MfD at the point of X-ray analysis. In addition, the focused beam spot has to be well defined (with a movable aperture) in order to not illuminate the side walls. These two steps would likely prevent this solution data disruption from Cu build-up on the internal surface of the device.

In this work, *X*-ray transparent polyimide film (Kapton®) layers were chosen to fabricate MfDs. The material was sourced commercially (Bevi AB, Sweden), and the thickness of the foil (Kapton® HN) was 125 μm for the fluidic path layer and 20 μm for the sealing layers (UL 510) on the top and bottom. The choice of polyimide was due to the thermal stability of the material (400°C), good mechanical properties [21] and X-ray compatibility. The film also has high transmission of X-ray frequencies and has, compared to other polymers, low sensitivity to ionising radiation damage [22].

The microfluidic pathway design was created using computer-aided-design (CAD) software (SOLIDWORKS 2018, Dassault Systèmes, France). The MfD was made of three separate polyimide layers with the middle fluidic layer (design from CAD) sealed on both sides. Three inlet channels (300 μm wide) and a central channel for the laminated flow (500 μm wide) were designed with a total length of 70 mm. To optimise the flow-focusing performance and the equal distribution of flow streams, the side (sheath) inlets were angled at 45° to the sample inlet. This angled setup also helped facilitate the tubing connectors and chip holder design - discussed in section 2.2.

X-ray Beam path Considerations for Device Design: The path length is the distance through the sample that the light has travelled (measured sample thickness) [5,23]. Figure 2 shows a simplified illustration of the path length calculation for different flow-focusing parameters, i.e., differing ratios of the sheath to sample thicknesses for the device(s) used in this study. The samples inside the channel were laminated with sheaths on both sides, usually DI water in this work. The sheaths, therefore, did have a small contribution to the attenuation of the beam when flown independently of samples in the channel. The choice of sheath also depends on the

viscosity comparable to that of the sample, thus avoiding any diffusion in the channel during pressure-driven flow.

As examples of the effect of sample and sheath fluid thicknesses, Figure 2 B shows a longer path length (~200 µm) but with a relatively smaller volume of the sample flow interacting with the X-ray beam. In this scenario, a very small proportion of the total volume of the sample is probed. Figure 2 C shows a smaller path length (~77 µm) but with a relatively larger volume of the sample interacting with the X-ray beam (NOTE flow direction of fluid is into the page). In this scenario, an increased proportion of the total sample volume is probed, and the sample material contact with the MfD is reduced.

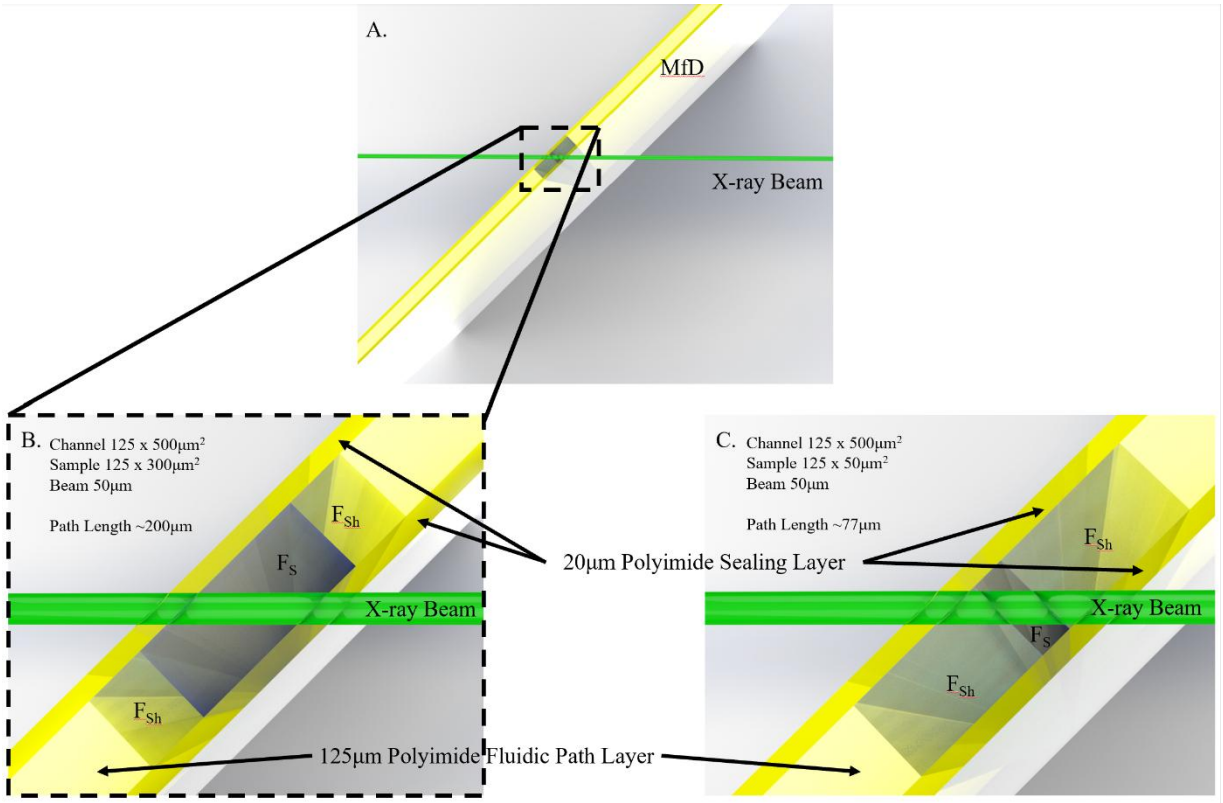


Figure 2 - Determination of tuneable sample width and path length. F_s and F_{Sh} are sample and sheath flow, respectively; the flow direction is into the page. The device channel is 500 µm wide and 125 µm deep (thickness of the Kapton device fluidic layer). The sheath and the sample flow completely fill the fluidic layer. The X-ray beam (Ø50 µm) interacts with the fluid sample at 45°. The figures illustrate the interaction between the X-ray

beam, MfD, sheath fluid and the sample fluid. A. shows a perpendicular cross-section of the MfD showing the fluidic path in the centre. In B. the maximum sample width (300 μm) is illustrated, resulting in ~200 μm pathlength for the beam through the sample. In C. the minimum sample width tested (50 μm) is illustrated, resulting in ~77 μm pathlength for the beam through the sample.

Different sample vs sheath widths were tested in this work, as they make up the total sample path length, placed at 45° to the *X*-ray beam and fluorescence detector. The signal-to-noise ratio (SNR) was used as a quality determinant for the data gathered from the MfDs using different fluidic layer thicknesses; see section 3.2.

Kapton Device Fabrication: The channels for the centre foil layer were cut using a laser-cutter (ÖSTLING Marking Systems GmbH, Germany, Class 2M LASER, wavelength 635 nm). The laser-cut layer was thoroughly rinsed in isopropyl alcohol (IPA) and dried with nitrogen gas to provide a clean bonding surface for sealing layers. Subsequently, the layer was sealed using a silicone adhesive coated Kapton tape (20 μm thick) on either side to complete the microfluidic chip (components 6, 7 and 8 in Figure). The device's sealing involves high levels of precision to manually press and roll the polyimide adhesive tape onto the laser cut polyimide fluidic layer to avoid any air pockets and misalignment issues. The connector layer (component 8 in Figure) involved an additional step. The inlets and outlet on the connector layer were punched with a biopsy punch of 1 mm diameter and then aligned appropriately to the underlying fluidic layer (component 7 in Figure). Once the chip was sealed, the connectors were fitted to the device using a bio adhesive tape (Adhesive ring - fluidic design 0698, from Microfluidic ChipShop, Germany). Standard male Luer or Labsmith fluid connectors were used (Fluidic 263, Microfluidic ChipShop, Germany or Bonded port connector LS-400 and One-piece fitting LS-T116-100, Mengle engineering respectively). To increase the rigidity of the thin Kapton

devices, a device holder and auxiliary assemblies were designed using CAD (components 1 and 10 in Figure). The fluidic connectors were inserted into the 3D printed female hollow ports (component 10 in Figure).

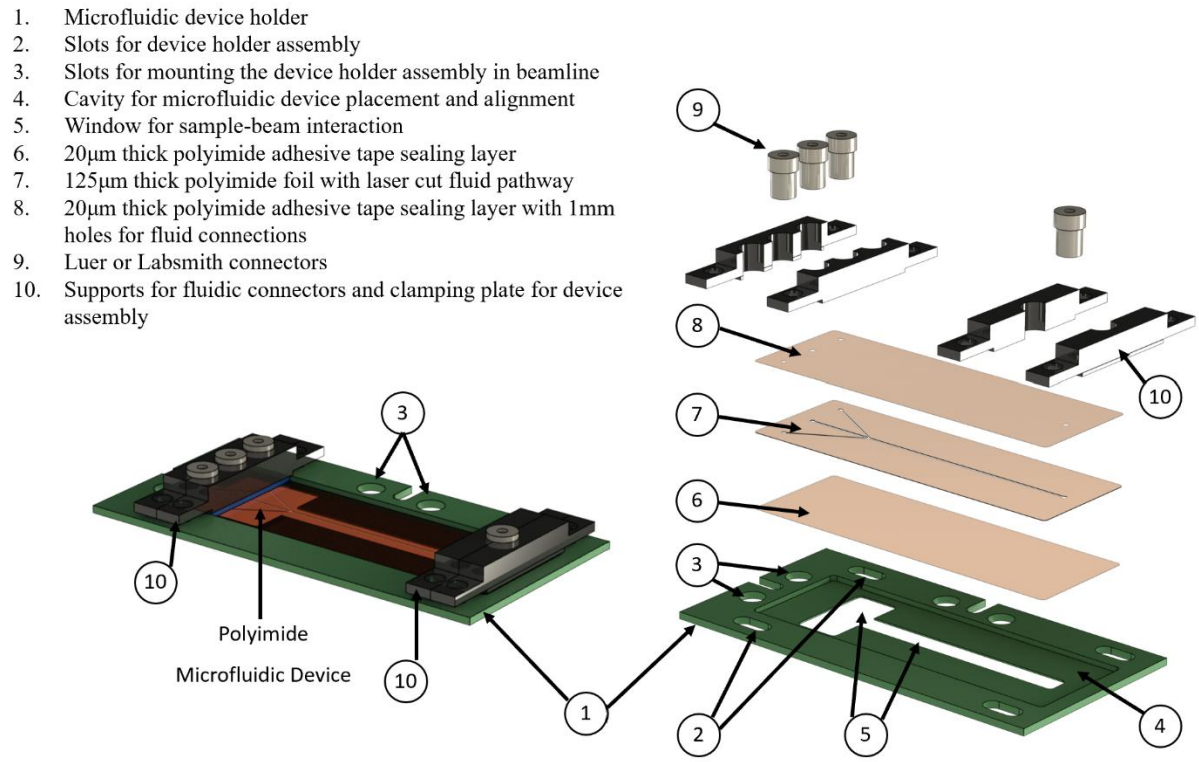


Figure 3 – (Left) Microfluidic device holder fully assembled with the device and fluidic connectors used at the beamline. (Right) Exploded view showing the various components of the device holder and the polyimide device

2.2 Device Holder Fabrication

The device holder plays a pivotal role in beamline-related studies as the experiments happen in an enclosed hutch with remote manipulation due to ionising radiation dangers from the X-ray beam usage. The thin polyimide MfDs required a robust backing to prevent device deformation during operation. The device and holder assembly were mounted vertically, hanging from the manipulation stage without support below (Figure 4, this is the sample setup used at the Balder beamline at MAX IV). The device holder was designed using CAD and fabricated either from a micromachined 3mm FR4 printed circuit board (PCB), or 3D Printed from continuous glass fibre reinforced nylon (Mark TWO, Markforged Inc., USA). The use of

two methods was for an additional study comparison of the stiffness and accuracy of the MfD device holder. The fluidic connector supports and clamping plates were 3D Printed from continuous glass fibre reinforced nylon (Mark TWO, Markforged Inc., USA). The layout of the device holder had a window (component 5 in Figure) to allow beam-sample interaction without blocking the incident and scattered beam with the 3D Printed material (this blocking would cause X-ray signal attenuation and possible measurement data corruption). The inlets and outlet were additionally supported with a pair of open blocks that appropriately position the Luer fittings (mentioned above) (components 12 and 13 in Figure). This need for additional support was due to the thinness of the device and the reason to place all the inlets/outlets on the same vertical plane to simplify the device holder design.

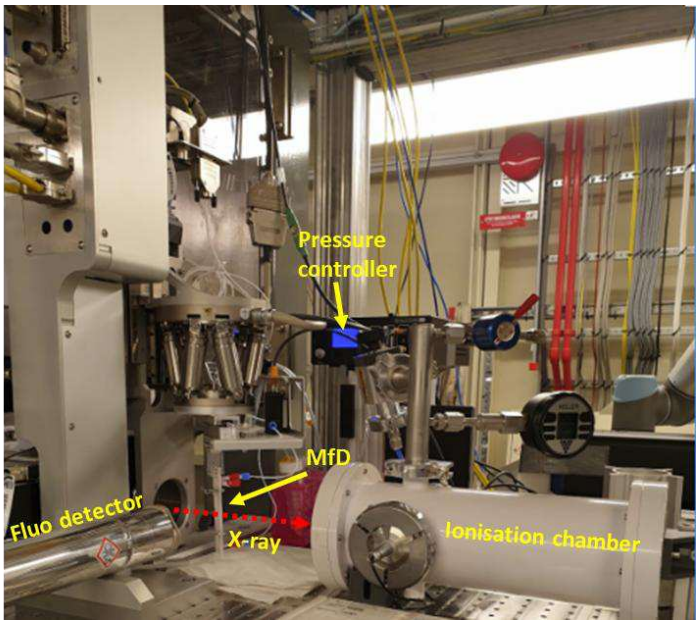


Figure 4 – Microfluidic device mounted in 'hanging mode' on the beamline stage fully assembled with holder, fluorescence detector and ionisation chamber.

2.3 Sample Delivery System

The sample delivery system determines the flexibility and pressure boundaries of the entire MfD and thus affects the performance in experiments in terms of interrupted flow patterns, unstable flow between different layers (sheath and sample), air bubbles and so on. The

experimental setup consisted of the following components: a pressure controller with four outlet channels of 0-200 mbar and 0-2 bar pressure ranges (MK3+ - OB1 from Elveflow, France); microfluidic flow rate sensors (MFS from Elveflow, France); and a microscope (Nikon Eclipse Ci – NIS-Elements BR 5.21.01) that was customised to visualise an MfD mounted vertically to the experimental bench. The pressure controller was supplied with N2 gas from a standard laboratory cylinder. Sample reservoirs of various sizes, e.g., Eppendorf tubes, Falcon tubes or glass bottles (Elveflow, France) were connected via ferrule and flange fittings; the research team's previous experience indicates that the reservoir container has no discernible effect on the performance of the system. Polytetrafluoroethylene (PTFE) tubing of 1/16" outside and 1/32" inside diameter (Elveflow, France) was experimentally determined to have optimal fluidic resistance for the MfD device in this study. The outlet from the MfD was connected to a waste collector (Falcon tube or beaker). The fluid control and actions were established using the microfluidic pump control software (ESI Microfluidic Software, Elveflow, France). The experimental setup is shown in Figure .

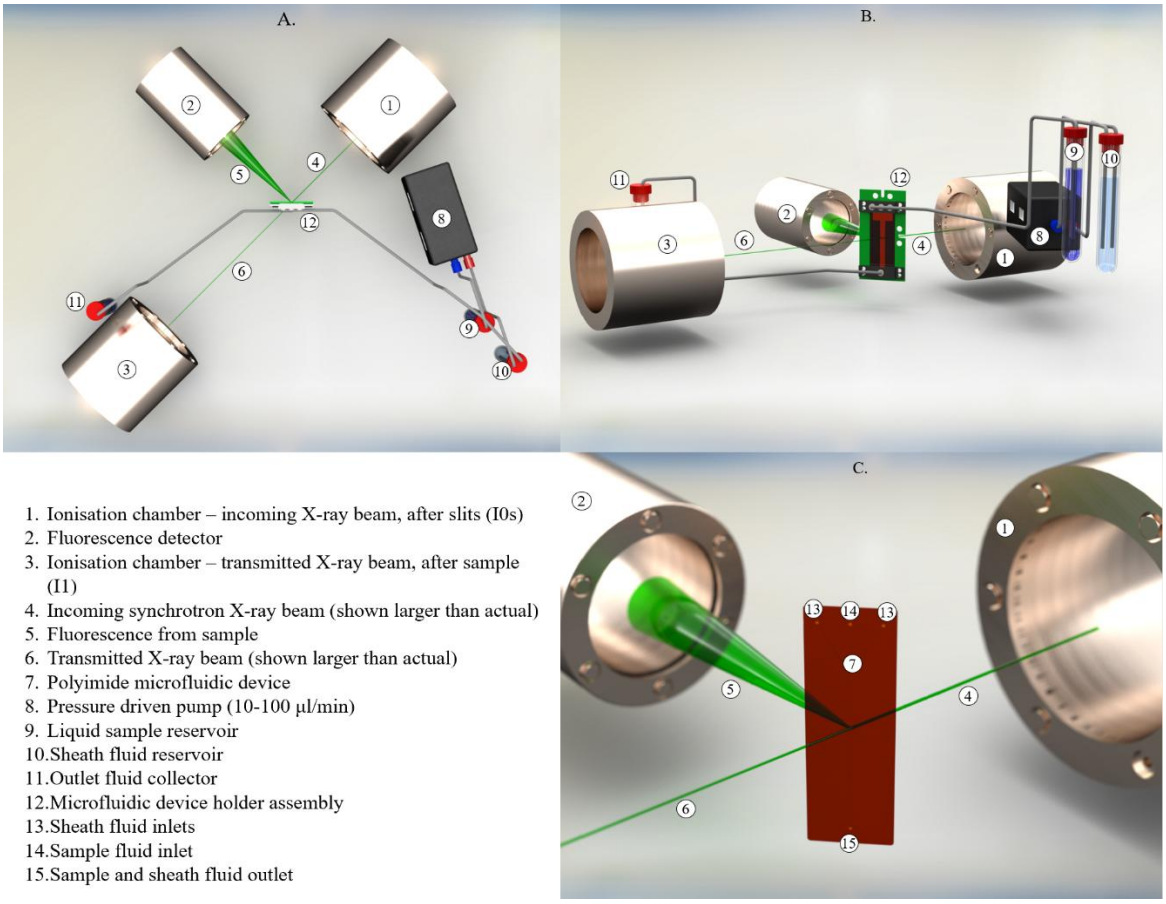


Figure 5 - Schematic of the experimental setup. A. Top view showing the path of the X-ray beam and detection in transmission (I1) and fluorescence; B. Side view showing the hydrodynamic flow-focusing microfluidic device and fluidic connections; C. Closeup of the polyimide device and X-ray beam interaction (holder and fluidic connectors hidden for clarity)

2.4 Sample Preparation and X-ray Data Collection

Sample preparation: Copper sulphate ($CuSO_4$) in water (180 mM) was used as the sample solution in this study to test the MfD device. The solution was degassed by sonication (15 minutes at 27°C) and filtered (0.2 µm, PTFE) through a syringe filter to remove any particles before being loaded into the sample containers (15 mL Falcon tube). Degassed purified Type 1 water (Milli-Q® IQ Water Purification System, Merck KGaA, Germany) was used for the sheath flow fluid via a 50 mL Falcon tube reservoir, connected to the pressure controller. All

sample preparation was performed at the MAX IV Biolab facilities. In this work, the sheath was degassed DI water (Table 1).

Table 1 - List of samples used in this study

Name	**Concentration**
$CuSO_4$(aq)	180 mM
Coomassie Blue	5 g in 50 mL of DI water
DI water	N/A

X-ray data collection: There are two modes of detection used at the Balder beamline, transmission and fluorescence. Transmission is the collection of spectra through the sample, which provides information on the absorption of intensity by the sample, and fluorescence is the spectral collection at 45°, which provides information on scattered light by the sample. The conditions for sample mounting at Balder with respect to the MfD and the sample source are the same as for previously published work [24]; the schematic setup is also shown in Figure .

XAS data were collected in fluorescence mode at the Balder beamline using the Silicon Drift Detector (SDD) (X-PIPS™ 7-element SDD, Mirion Technologies Inc., USA). The liquid nitrogen (LN2) cooled double crystal (Si111) monochromator (FMB Oxford, UK) was calibrated to 8979 eV for the first inflexion point of the Cu-foil for the copper *K*-edge data collection. The focused *X*-ray beam (50 x 50 μm^2) passed through an aperture of movable slit blades set to vertical 300 μm x horizontal 150 μm opening, restricting the final beam dimensions. The beam's shaping was made to ensure that no part of the beam's weaker "tails"

would move onto the channel walls (channel width 500 μm). The hydrodynamically focused channel of the MfD was aligned to the beam position by horizontally scanning over the channel.

During the experiments, the samples were flowed through the three inlet microchannels at rates between 30 μl/min and 150 μl/min to tune the width of the middle sample flow within the sheath flows. At energy above the absorption edge of interest, the fluorescence counts/sec were checked, and the region of interest (ROI) was set around the emission line of interest (Cu Kα). The distance between the sample and the fluorescence detector was adjusted to be in the linear response range.

Continuous fly scans to record Extended X-ray Absorption Fine Structure (EXAFS) (settings: Δt 10 ms, energy step 0.25 eV, -150 to +650 eV around E0, ~100 sec/scan) or only X-ray Absorption Near Edge Structure (XANES) (settings: Δt 10 ms, energy step 0.25 eV, -80 to +150 eV around E0, 33 sec/scan) were started when the sample was confirmed in the channel by checking the increase in Cu fluorescence count. The number of scans is indicated in each figure (Figure 9-11). E0 in this case, was the tabulated edge energy of elemental Cu *K* 8979 eV.

The multiple scan repeats of the sample solution (

Table 1) were first examined for changes in the edge region; if no changes were observed, they were merged into a single averaged spectrum. The spectrum normalisation and extraction of EXAFS oscillations and conversion of the energy scale to the wave-vector (k) scale were performed as previously described [25]. Fourier Transforms (FT) of EXAFS spectra were calculated using in-house software and $\cos^2$ windows extending over 10% at both k-range ends

(k = 2–13 $Å^{-1}$). No simulation of EXAFS was attempted, only the visual inspection compared to Cu foil EXAFS and comparison of signal to noise were evaluated.

3 Results and Discussion

3.1 Device Characterisation

The devices were fabricated in Kapton (polyimide) with the techniques mentioned in section 2.1, and assembled within the chip holder (Figure 6). The chip holder provided a robust backing to the Kapton devices throughout the experiment that lasted for more than 24 h.

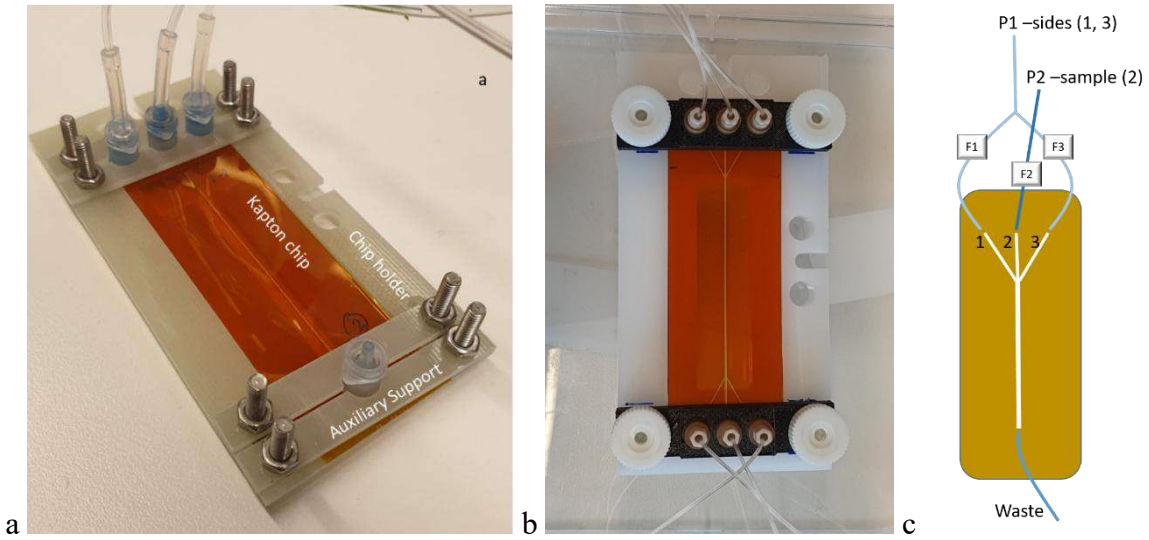


Figure 6 - Fabricated Microfluidic Devices in holder. a) Kapton chip mounted on chip holder, Luer connectors, Silicone sleeves and Teflon tubing; b) Kapton chip with trifurcation outlet for future sample recovery, Labsmith connectors and tygon tubing; c) A schematic of the MfD with labelled inlet channels (1, 2, 3), applied pressure (P1, P2), flow sensors (F1, F2, F3) and waste, nomenclature used throughout the paper.

Relative Sheath and Sample Flow Rate: The ratio between sheath and sample flow rates influenced the flow focusing capability of the device in terms of the sample width and mixing of solutions. The effect of flow rate ratio *k* can be defined as the ratio between the flow rate of side flows (sheath) to the central channel (sample), given by

$$k = \frac{V_{sheath}}{V_{sample}} \qquad (1)$$

Where V_{sheath} and V_{sample} are volumetric flow rates of sheath (on both sides) and sample flows, respectively.

Several experiments were conducted to determine the sample width when flow rates (based on pressure values) on sheath and sample were changed accordingly. Based on the mathematical k-value, the pressure values were chosen to determine the sample widths. This was done to predict the sample width at the beamline where there is no access to image the sample flow due to space constraint. The same sample width can be achieved by balancing the pressures/flows of sheath and sample (**Error! Reference source not found.**). It was also observed that the sample fluid width decreased as the flow rate of the sheath fluid increased over that of the sample fluid (eqn. 1). The offline experiments provided a guideline to predict the width of the focused sample stream at the beamline and therefore the pressure ranges read remotely via the software helped us to get a fair idea whether the sample width was greater than the beam size (Figure 7). Multiple tests revealed a pattern of flow rate *vs.* sample width relationship (Figure 88).

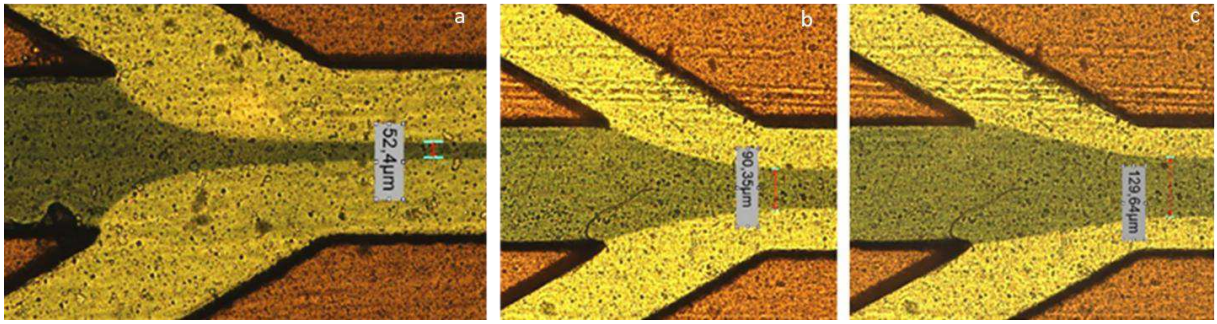


Figure 7 - Images of MfD when flowing Coomassie dye with DI water in the central channel and DI water on side channels at different pressure values (flow rates), resulting in different sample widths. When sample fluid

pressure increases above the sheath fluid flow, the sample fluid stream width increases. a) side flow 80 mbar and central flow 68 mbar; b) side 79 mbar and central 80 mbar; c) side 70 mbar and central 80 mbar.

***Tuneable Sample Width**:* The optical characterisation of the MfD was carried out at the offline station microscope. The device characterisation was done to validate the device's performance under different pressure and flow rate conditions. The devices were tested with deionised water (DI) and Coomassie blue dye (Table 1, Coomassie Brilliant Blue G-250 Dye, Catalog# 20279 from Thermo Scientific™, Sweden). A dye and DI water solution was prepared, filtered and degassed before flowing through the setup. Several tests were done for different pressure values on the P1 (side pressure) and P2 (sample pressure) to tune the sample widths (Figure 8, Graph 1a).

Table 2 - Applied side pressure P1, applied sample pressure P2, measured sample width with microscope. Linear fitting of the pressure values for each sample width gave a (intercept) and b (slope) parameters, see graph 1a

P1 (mbar)	P2 (mbar)	Sample width (µm)	Sample flow rate (µm/min)
30	22.5	100	65
60	47	100	103
90	73	100	141
30	24	118	84
60	52	118	144
90	81	118	186
30	26	149	95
60	52	149	144
90	81	149	186
30	29	200	121
90	88	200	234

30	37	300	183
90	107	300	400

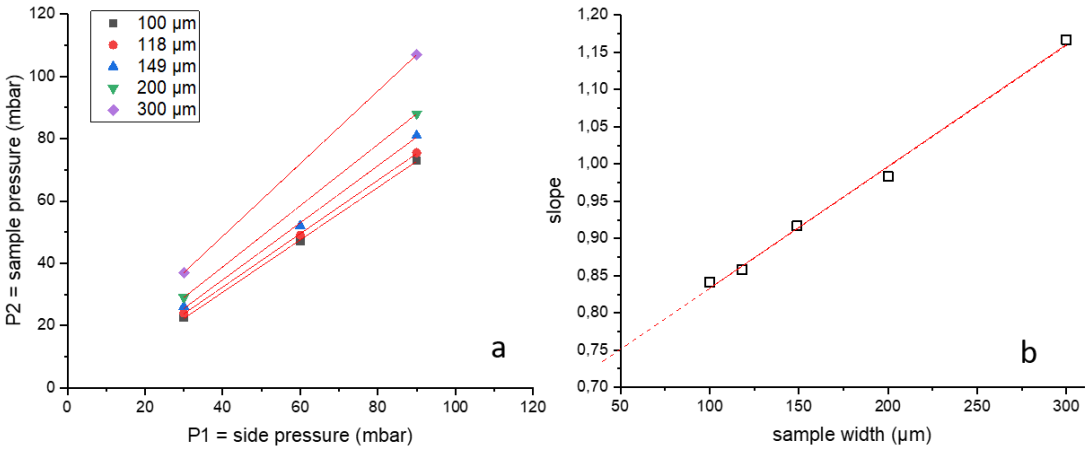


*Figure 8 - a) A sample pressure (P2) versus side pressure (P1) for sample widths of 100 (square), 118 (red circle), 149 (blue up triangle), 200 (green down triangle), and 300 µm (purple diamond) with linear regression fit (red line); b) Slope values from fits in "a" versus the measured sample width. Linear regression line (slope = 0.669 + 0.00164 *sample width) from this plot was used to predict the slope at any width to calculate the pressures P1 and P2 from the formula P2 = -2 + slope*P1.*

P2 was plotted *vs.* P1 with a linear relationship for each sample width (Figure 8, Graph 1a). The slope grew bigger the wider the sample, while the intercept was ~ -2. In a second linear regression plot (Figure 8, Graph 1b) the slopes were plotted versus the sample widths to predict the slope for any desired sample width within the range of 50 -300 µm. By first calculating the slope (slope= 0.669 + 0.00164 * sample width) and then use the slope value to predict the needed sample pressure (P2) for a chosen P1 side pressure (P2 = -2 + slope*P1). In this way, without access to a microscope the sample width for the experiment at the beamline was predicted.

3.2 Device characterisation with X-rays

Validation of sample width with X-rays: Validation of the "sample width predictor" method, described above, was performed using X-rays to indirectly measure the sample width from the Cu fluorescence signal detected from the sample copper sulphate solution. The MfD was horizontally scanned across the fluidic channel by moving the x-axis motor position (the MfD is attached to the sample positioning system) in front of the X-ray beam. Fluorescence counts recorded and plotted *vs.* the x-axis position in mm gave a peak spectrum (Figure 9, graph a). The full width half maximum (FWHM) of the fitted peak represents the hypotenuse in a right-angled triangle with the legs being the real sample width and the device thickness, depicted by the inset in Figure 99 (graph a). Using the Pythagoras theorem, the sample width was calculated.

In Table 3, the calculated and applied pressures for the sample widths 50, 100, 150 and 200 μm were compared to the resulting flow meter measured flows (F1 (sheath), F2 (sample), and F3 (sheath)) and X-ray measured sample widths based on the FWHM described above. The intended sample width (in the first column) was not in complete agreement with the measured sample width (5^{th} column) 50 became 69, 100 became 115, 150 became 124 and 200 became 131 μm wide samples. The 50 and 100 μm became bigger, and the 150 and 200 μm became smaller than predicted, with an increasing uncertainty the closer to the lowest and highest numbers. In the last column, the signal intensity from the sample under the different conditions is given as fluorescence counts with the ratio of the Cu region of interest versus the total. The wider the sample, the more counts hitting the detector are Cu fluorescence.

Table 3 - Summarising the metrics corresponding to the different experimental conditions related to sample width calculated and measured.

Calculated* Sample width (µm)	Set P1 (mbar)	Set P2 (mbar)	Measured flows (F1, F2, F3) (µl/min)	Measured* * Sample width (FWHM) (µm)	Fluo kcounts *** (Cu roi/tot)
50	30	21	150/32/137	69 (143)	35/306 (11%)
100	30	23	113/65/150	115 (170)	78/390 (20%)
150	30	26	90/85/127	124 (176)	106/432 (24%)
200	30	28	104/93/98	131 (181)	128/438 (29%)

* Calculated based on a linear regression analysis of the slope of pressures vs sample widths, see text.

** Using Pythagoras theorem: FWHM of fluorescence peak in channel cross-section (motor x) is the hypotenuse, and device thickness (125 µm) is leg b, and sample width is leg a.

*** Fluorescence detector counts at the sample peak (Figure 9) motor position, in the region of interest (Cu Kα) and the total count number, percent Cu counts in parenthesis.

Signal quality under flow: The quality of XAS data versus sample width and sample consumption was judged by recording XANES and EXAFS scans under the four chosen conditions described in **Error! Reference source not found.**, hereafter referred to as the sample pressure, P2, 28, 26, 23 and 21 mbar. In Figure 9b, the Cu XANES is displayed with acceptable quality in all four cases, but not surprisingly, with better signal to noise (Table 3) in the widest sample (28 mbar). Quality can be increased by measuring for a longer time/with more repeats; however, this will consume increasing sample volume. In this example, eight repeats were averaged to give a total scan time of ~5 minutes, which consumed between 160-465 µL of sample for the different pressures, see **Error! Reference source not found.**. To judge the quality of EXAFS (Figure 99c), the oscillations were compared to "average" EXAFS composed of 48 scan repeats. In this averaged EXAFS, oscillations are distinct until k-11, where they quickly lose intensity. In the test case of 8 scans (14 minutes), all pressures displayed distinct oscillations up to k-10. However, only P2 28 and 26 mbar showed the last

oscillation as discernible from the noise. As with previous cases, the data quality improves with additional repeats, but this consumes a larger sample volume. The consumption of the sample for the data collection at P2 28 mbar (1240 µL) compared to P2 21 mbar (430 µL) was almost three times higher (**Error! Reference source not found.**). This is not particularly a problem with samples of low-cost and abundance, like the copper sulphate test sample. However, the sample used in the analysis can often be both costly and rare; therefore, better data collection with smaller sample consumption is preferable.

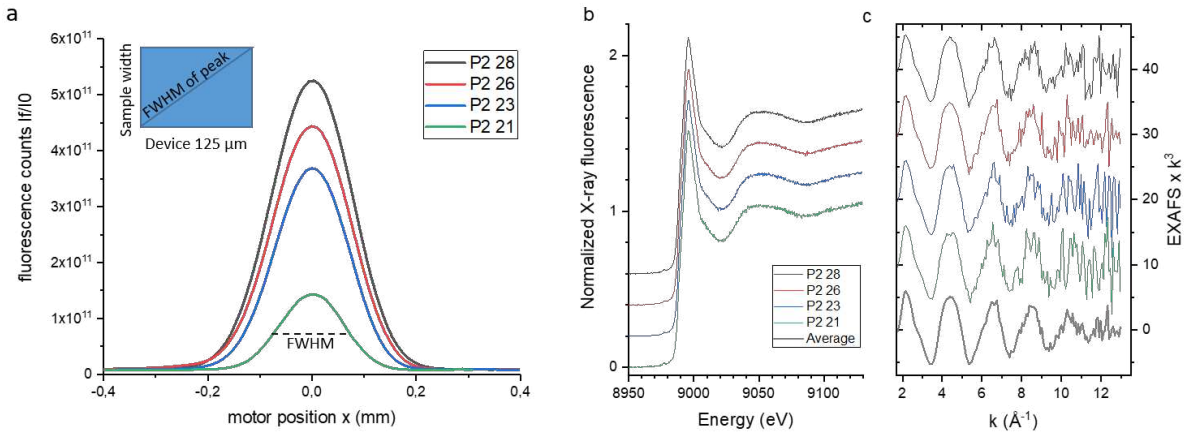


Figure 9 - Four different P2 pressures (sample channel) were investigated 28 (black), 26 (red), 23 (blue) and 21 mbar (green). In a) the sample width was measured via the lateral scanning motor position x versus the fluorescence count rate on the detector normalised to the incoming beam (I0). The peak's full width half maximum (FWHM) relates to the actual sample width, as illustrated in the top left corner. b) Cu K-edge XANES spectra of the 180 mM $CuSO_4$(aq) solution (average of 8 scan repeats at 35 sec/scan, total ~5 min/XANES). c) Displays extracted k^3 weighted EXAFS oscillations recorded under the same conditions (8 scans at 100 sec/scan, total ~14 min/EXAFS) and compared to the average curve of 48 scans recorded under different pressure settings (grey, total scan time 80 min).

Table 4 - Statistics and sample consumption for XANES and EXAFS data collection at different P2 (sample pressure), which translates to different sample channel width given in Table 3.

Set P2 (mbar)	XANES (S/N, 8910-8930 eV max-min, (weight))	Sample volume spent for XANES (5 min x flow) (µL)	Sample volume spent for EXAFS (14 min x flow) (µL)
21	751 (0.26)	160	430
23	1139 (0.61)	325	870
26	1396 (0.92)	425	1130
28	1457 (1)	465	1240

Static sample, reduction and diffusion: Radiation damage on the static sample inside the channel was investigated. The flow stopped, and repeated EXAFS spectra were recorded continuously for 37 minutes (22 scans, Figure 10). The pre-edge structure increased from the third scan onwards, indicating Cu^{II} → Cu^{I} reduction. In addition, after 13 minutes, the fluorescence intensity dropped (scan 8) significantly and continued dropping until scan 10. The authors attribute this drop to be likely due to diffusion of the Cu from the sample stream into the sheath flow stream, diluting the Cu signal during static interaction. From scan 11 the intensity increased again, but the edge was strongly shifted to lower energy, and a shoulder feature arose. The shape stayed for the next 11 scans (scan 11-22), but the intensity grew, likely showing deposition of "Cu" invigorate on the MfD device. To learn more about the nature of this deposit, the extracted EXAFS oscillations were analysed and the FT of the initial first two scans and the deposit scans were compared to both the flow EXAFS (same "average" as in Figure 910c) and a Cu foil (Figure). In the deposit EXAFS spectrum (Figure 11a, black), the EXAFS oscillation amplitude underwent destructive interference. In the resulting FT of EXAFS, the two FT peaks at around 4-5 Å reduced in distance (arrows, Figure b), resembling the Cu-Cu distances found in metal foil (dashed line). These data are consistent with radiolysis-

driven conversion of solvated Cu^{II} to reduced copper species under static irradiation. The appearance of Cu^0-like EXAFS features in the deposit does not, by itself, prove a direct Cu^I-to-Cu^0 photoreduction pathway, because aqueous Cu^I can also undergo disproportionation to Cu^{II} and Cu^0. We therefore interpret the deposit more cautiously as a copper-containing reduced phase formed during beam exposure, plausibly via Cu^I intermediates followed by disproportionation and/or precipitation at the channel window [5,26]. The reducing equivalents are generated by water radiolysis in the X-ray beam.

The Cu^{II} reduction process is similar to what happened in the experiments with single sample channel flow in the COC device without flow focusing (Figure S1). From these tests for radiation-sensitive liquid samples, one needs to flow the sample and use the hydrodynamic focusing strategy to get chemically sound results.

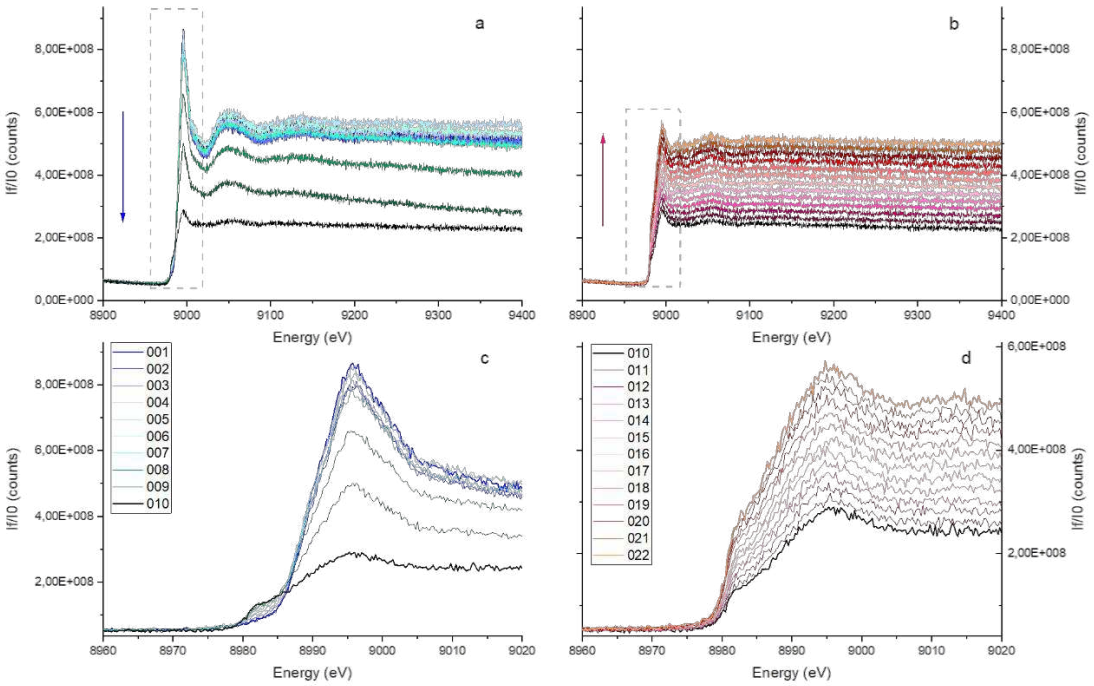


Figure 10 - Following the evolution of EXAFS scans after the fluid flow is stopped inside the device observation channel during a time of ~37 min, each scan repeat was ~100 sec. On the y-axis, fluorescence counts (If) are divided by the incoming X-ray beam (I0), but not normalised to 1, for comparison of signal strength. In a) and c) scan repeats 1 to 10 are displayed, with the dashed box in a marking the energy range in c. The same is true for b) and d), but displaying scan repeats 10-22.

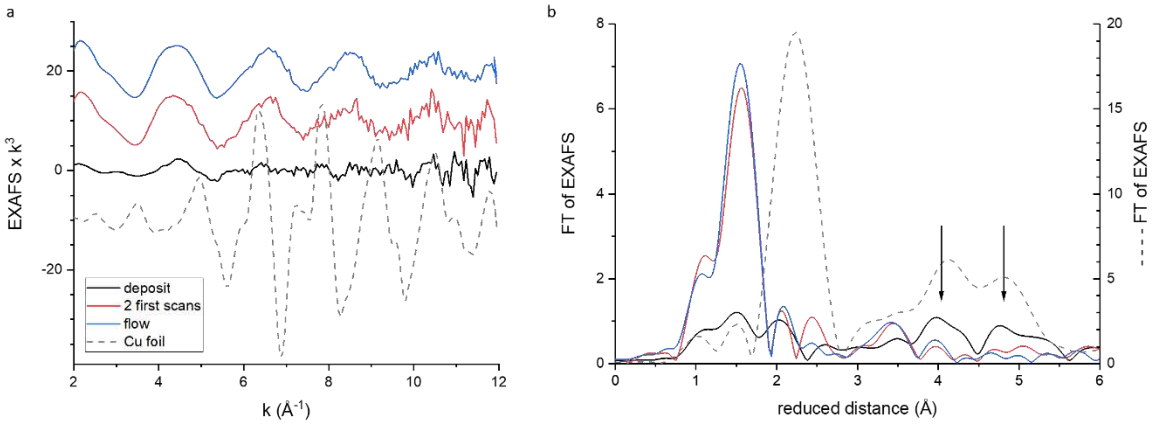


Figure 11 - a) Extracted EXAFS oscillations (k-range 2-12 Å^{-1}, k^3-weighted) from the static experiment in graph 3, average of the two first scans before change of spectrum (red) and average of the deposit scans 10-22 (black) compared to the average flow (blue) and the Cu foil EXAFS (dashed grey), y-axis is offset for clarity. b) Fourier transform of EXAFS with two arrows marking the long-range Cu-Cu distances in the metal foil. The dashed line for the Cu foil has its y-axis to the right and the solution samples have the scale to the left.

3.3 Bubbles in Fluidic Devices

When water is exposed to an intense X-ray beam, bubbles are formed. These bubbles are an obstacle in any microfluidic platform, as the design and flow pattern can be disrupted by bubble formation and retention. Additionally, as XAS is a sensitive analytical method, bubbles are obviously evident in the spectra obtained. In the presented work, the aqueous solutions and sheath flows with DI water were continuously flowed with flow rates (sheath> 110 µl/min and sample > 30 µl/min) that avoided any bubble formation during the measurements. Acquiring spectra on continuous flow of aqueous solutions using hydrodynamic flow focusing proved an effective method to avoid bubble formation that is otherwise inevitable in static X-ray measurements.

A limitation of the present study is that the device is validated using a benchmark aqueous $CuSO_4$ system rather than a chemically complex or application-driven case study. We view this as an intentional methodological step: Cu K-edge XAS provides a sensitive readout of

beam-induced redox chemistry, making it an appropriate system for establishing the platform's operating window. Future work should extend the device to lower-concentration samples, multicomponent solutions, time-resolved reaction chemistry and biologically or catalytically relevant metal systems, where the combination of radiation-damage mitigation and low sample consumption is expected to be especially beneficial.

4 Conclusion

In this study, fabrication and characterisation of a Polyimide microfluidic platform that can be used successfully with a Synchrotron Hard *X*-ray Absorption Spectroscopy technique to study aqueous salt solutions is presented.

Investigating metal ion coordination in solution via XAS has become more efficient with modern synchrotron beamlines, yet high flux X-rays can cause sample degradation during static exposures. Microfluidic flow devices provide constant replenishment of fresh samples to prevent X-ray-induced redox processes, resulting in bubble formation and elevated temperatures. This study utilised hydrodynamic flow focusing of $CuSO_4$ in aqueous solutions using a custom-designed polyimide MfD. Although holding only minimal sample volumes, it was demonstrated that sufficient signal strengths could be obtained by directing the X-ray beamline at an angle through the transparent microfluidic channel.

The fabrication of the device is low cost, and it can be operated with commercial microfluidic pumps and control thus lending itself well for exploitation also at other X-ray beamlines. The Polyimide film displayed low background signal and negligible attenuation to the measurements taken throughout the study, showing potential of such a setup for applications related to e.g. catalysis studies or life science applications. The continuous flow of the sheathed sample demonstrated several benefits. First, it avoided sample build-up at the device wall and subsequent metal reduction, a process that may interfere with measurements using this device,

setup and sample. Second, bubble formation was avoided at flow rates of 30 µl/min and above. Finally, continuous flow of the sample in a narrow flow stream allowed utmost of the sample to be used in the analysis thus making the process more efficient. Flowing the aqueous sample provided better quality of spectra than measuring on static sample due to chemical changes and bubbles formed in the beam path. The quality depends on the homogeneity of the XAS sample, a true solution is 100% homogenous and therefor tend to yield better quality data than heterogenous powder samples.

Cu redox chemistry is often an important component in the catalysis industry (e.g., click chemistry) as well as in biology (over thirty Cu containing enzymes). In other words, Cu is a key target for XAS analysis. Therefore, findings here have wider implications and benefit to hard X-ray spectroscopy outside of the use of aqueous $CuSO_4$ solution. In addition, many other radiation sensitive systems and water-based liquids are studied with X-rays techniques, where conclusions from this work could impact the choice of device and design.

Acknowledgements

We gratefully acknowledge that this project is financially supported by the Swedish Foundation for Strategic Research, grant ITM-0375. The MAX IV Laboratory, Lund University, is acknowledged for allocation of beamtime at the Balder beamline for these studies (in-house research proposal 20200545). Research conducted at MAX IV, a Swedish national user facility, is supported by the Swedish Research council under contract 2018-07152, the Swedish Governmental Agency for Innovation Systems under contract 2018-04969, and Formas under contract 2019-02496. Microfabrication was performed by the Customized Microfluidics SciLifeLab-Uppsala University local unit using the MyFab-Uppsala cleanroom. Myfab is funded by the Swedish Research Council (2019-00207) as a national research infrastructure.

Data availability

The datasets generated during this study, including the processed XANES and EXAFS spectra, beamline metadata, pressure/flow calibration data, and the CAD files required to reproduce the microfluidic device and holder geometry, will be deposited in a public repository before publication. The accession link will be added at proof stage. Until then, the data are available from the corresponding authors upon reasonable request.

Funding Declaration

This work was financially supported by the Swedish Foundation for Strategic Research under grant ITM-0375. The authors acknowledge MAX IV Laboratory, Lund University, for the allocation of beamtime at the Balder beamline for these studies under in-house research proposal 20200545. Research conducted at MAX IV, a Swedish national user facility, was supported by the Swedish Research Council under contract 2018-07152, the Swedish Governmental Agency for Innovation Systems under contract 2018-04969, and Formas under contract 2019-02496. Microfabrication was performed by the Customized Microfluidics SciLifeLab-Uppsala University local unit using the MyFab-Uppsala cleanroom. Myfab is funded by the Swedish Research Council as a national research infrastructure under grant 2019-00207.

References

(1) Chantler, C. T.; Bunker, G.; D'Angelo, P.; Diaz-Moreno, S. X-Ray Absorption Spectroscopy. *Nature Reviews Methods Primers* **2024**, *4* (1). https://doi.org/10.1038/s43586-024-00366-8.

(2) Klementiev, K.; Norén, K.; Carlson, S.; Sigfridsson Clauss, K. G. V.; Persson, I. The BALDER Beamline at the MAX IV Laboratory. *J. Phys. Conf. Ser.* **2016**, *712* (1), 012023. https://doi.org/10.1088/1742-6596/712/1/012023.

(3) Mesu, J. G.; Beale, A. M.; De Groot, F. M. F.; Weckhuysen, B. M. Probing the Influence of X-Rays on Aqueous Copper Solutions Using Time-Resolved in Situ Combined Video/X-Ray Absorption near-Edge/Ultraviolet-Visible Spectroscopy. *J. Phys. Chem. B* **2006**, *110* (35), 17671–17677. https://doi.org/10.1021/JP062618M.

(4) Köster, S.; Pfohl, T. X-Ray Studies of Biological Matter in Microfluidic Environments. *Modern Physics Letters B* **2012**, *26* (26). https://doi.org/10.1142/S0217984912300189.

(5) Ekanayake, R. S. K.; Streltsov, V. A.; Best, S. P.; Chantler, C. T. Using XAS to Monitor Radiation Damage in Real Time and Post-Analysis, and Investigation of Systematic Errors of Fluorescence XAS for Cu-Bound Amyloid-β. *J. Appl. Crystallogr.* **2024**, *57* (Pt 1), 125–139. https://doi.org/10.1107/S1600576723010890.

(6) Qureshi, M.; Nowak, S. H.; Vogt, L. I.; Cotelesage, J. J. H.; Dolgova, N. V.; Sharifi, S.; Kroll, T.; Nordlund, D.; Alonso-Mori, R.; Weng, T. C.; Pickering, I. J.; George, G. N.; Sokaras, D. Sulfur Kβ X-Ray Emission Spectroscopy: Comparison with Sulfur K-Edge X-Ray Absorption Spectroscopy for Speciation of Organosulfur Compounds. *Physical Chemistry Chemical Physics* **2021**, *23* (8), 4500–4508. https://doi.org/10.1039/d0cp05323f.

(7) Nagasaka, M.; Yuzawa, H.; Takada, N.; Aoyama, M.; Rühl, E.; Kosugi, N. Laminar Flow in Microfluidics Investigated by Spatially-Resolved Soft X-Ray Absorption and Infrared Spectroscopy. *J. Chem. Phys.* **2019**, *151* (11). https://doi.org/10.1063/1.5115191.

(8) Probst, J.; Borca, C. N.; Newton, M. A.; van Bokhoven, J.; Huthwelker, T.; Stavrakis, S.; deMello, A. In Situ X-Ray Absorption Spectroscopy and Droplet-Based Microfluidics: An Analysis of Calcium Carbonate Precipitation. *ACS Measurement Science Au* **2021**, *1* (1), 27–34. https://doi.org/10.1021/acsmeasuresciau.1c00005.

(9) Brenker, J.; Henzler, K.; Borca, C. N.; Huthwelker, T.; Alan, T. X-Ray Compatible Microfluidics for in Situ Studies of Chemical State, Transport and Reaction of Light Elements in an Aqueous Environment Using Synchrotron Radiation. *Lab Chip* **2022**, *22* (6), 1214–1230. https://doi.org/10.1039/d1lc00996f.

(10) Levenstein, M. A.; Chevallard, C.; Malloggi, F.; Testard, F.; Taché, O. Micro- and Milli-Fluidic Sample Environments for in Situ X-Ray Analysis in the Chemical and Materials Sciences. *Lab Chip* **2025**, *25* (5), 1169–1227. https://doi.org/10.1039/d4lc00637b.

(11) Mesu, J. G.; Van Der Eerden, A. M. J.; De Groot, F. M. F.; Weckhuysen, B. M. Synchrotron Radiation Effects on Catalytic Systems As Probed with a Combined In-Situ UV−Vis/XAFS Spectroscopic Setup. *Journal of Physical Chemistry B* **2005**, *109* (9), 4042–4047. https://doi.org/10.1021/JP045206R.

(12) Nienaber, K. H.; Nehzati, S.; Cotelesage, J. J. H.; Pickering, I. J.; George, G. N. X-Ray-Induced Photoreduction of Hg(II) in Aqueous Frozen Solution Yields Nearly Monatomic Hg(0). *Inorg. Chem.* **2018**, *57* (14), 8205–8210. https://doi.org/10.1021/acs.inorgchem.8b00694.

(13) Garman, E. F.; Weik, M. Radiation Damage to Biological Samples: Still a Pertinent Issue. *J. Synchrotron Radiat.* **2021**, *28* (Pt 5), 1278. https://doi.org/10.1107/S1600577521008845.

(14) Berlanda, S. F.; Breitfeld, M.; Dietsche, C. L.; Dittrich, P. S. Recent Advances in Microfluidic Technology for Bioanalysis and Diagnostics. *Anal. Chem.* **2021**, *93* (1), 311–331. https://doi.org/10.1021/ACS.ANALCHEM.0C04366.

(15) Latypov, Z. Z. Flow-type cuvette of an optical analyzer with hydrodynamic focusing of the liquid under study. *Med. Tekh.* **1983**, No. 3, 31–32.

(16) Simonnet, C.; Groisman, A. Two-Dimensional Hydrodynamic Focusing in a Simple Microfluidic Device. *Appl. Phys. Lett.* **2005**, *87* (11). https://doi.org/10.1063/1.2046729/328437.

(17) Golden, J. P.; Justin, G. A.; Nasir, M.; Ligler, F. S. Hydrodynamic Focusing--a Versatile Tool. *Anal. Bioanal. Chem.* **2012**, *402* (1), 325–335. https://doi.org/10.1007/S00216-011-5415-3.

(18) Riordon, J.; Nash, M.; Calderini, M.; Godin, M. Using Active Microfluidic Flow Focusing to Sort Particles and Cells Based on High-Resolution Volume Measurements. *Microelectron. Eng.* **2014**, *118*, 35–40. https://doi.org/10.1016/J.MEE.2014.02.003.

(19) Lee, G. Bin; Chang, C. C.; Huang, S. Bin; Yang, R. J. The Hydrodynamic Focusing Effect inside Rectangular Microchannels. *Journal of Micromechanics and Microengineering* **2006**, *16* (5), 1024. https://doi.org/10.1088/0960-1317/16/5/020.

(20) Ha, B. H.; Lee, K. S.; Jung, J. H.; Sung, H. J. Three-Dimensional Hydrodynamic Flow and Particle Focusing Using Four Vortices Dean Flow. *Microfluid. Nanofluidics* **2014**, *17* (4), 647–655. https://doi.org/10.1007/S10404-014-1346-6/METRICS.

(21) DuPont: “Dupont Kapton Polyimide Film General Specifications”, Bulletin GS-96-7.

(22) Megusar, J. Low Temperature Fast-Neutron and Gamma Irradiation of Kapton® Polyimide Films. *Journal of Nuclear Materials* **1997**, *245* (2–3), 185–190. https://doi.org/10.1016/S0022-3115(97)00012-3.

(23) IMAMURA, R.; MIKAMI, K.; MINAMI, Y.; KANNO, I.; OHTAKA, M.; HASHIMOTO, M.; ARA, K.; ONABE, H. Unfolding Method with X-Ray Path Length-Dependant Response Functions for Computed Tomography Using X-Ray Energy Information. *J. Nucl. Sci. Technol.* **2010**, *47* (11), 1075–1082. https://doi.org/10.1080/18811248.2010.9711672.

(24) Micheal Raj, P.; Barbe, L.; Andersson, M.; De Albuquerque Moreira, M.; Haase, D.; Wootton, J.; Nehzati, S.; Terry, A. E.; Friel, R. J.; Tenje, M.; Sigfridsson Clauss, K. G. V. Fabrication and Characterisation of a Silicon-Borosilicate Glass Microfluidic Device for Synchrotron-Based Hard X-Ray Spectroscopy Studies. *RSC Adv.* **2021**, *11* (47), 29859–29869. https://doi.org/10.1039/D1RA05270E.

(25) Newville, M. Fundamentals of XAFS. *Rev. Mineral. Geochem.* **2014**, *78* (1), 33–74. https://doi.org/10.2138/RMG.2014.78.2.

(26) Johnson, D. K.; Stevenson, M. J.; Almadidy, Z. A.; Jenkins, S. E.; Wilcox, D. E.; Grossoehme, N. E. Stabilization of Cu(I) for Binding and Calorimetric Measurements in Aqueous Solution. *Dalton Transactions* **2015**, *44* (37), 16494–16505. https://doi.org/10.1039/c5dt02689j.